AGU PUBLICATIONS

JGR

Journal of Geophysical Research: Earth Surface

RESEARCH ARTICLE

10.1002/2014JF003132

Key Points:
- Ice viscoelasticity is important to the dynamics of ice stream stick slip
- Time-averaged contribution of stick-slip motion is similar to steady ice flow
- Ice viscosity is relevant in use of stick-slip observations for basal inference

Supporting Information:
- Readme
- Text S1

Correspondence to:
D. N. Goldberg,
dan.goldberg@ed.ac.uk

Citation:
Goldberg, D. N., C. Schoof, and O. V. Sergienko (2014), Stick-slip motion of an Antarctic Ice Stream: The effects of viscoelasticity, *J. Geophys. Res. Earth Surf.*, *119*, 1564–1580, doi:10.1002/2014JF003132.

Received 21 FEB 2014
Accepted 14 JUN 2014
Accepted article online 18 JUN 2014
Published online 16 JUL 2014

Stick-slip motion of an Antarctic Ice Stream: The effects of viscoelasticity

D. N. Goldberg[1], C. Schoof[2], and O. V. Sergienko[3]

[1]School of GeoSciences, University of Edinburgh, Edinburgh, UK, [2]Department of Earth, Ocean and Atmospheric Sciences, University of British Columbia, Vancouver, British Columbia, Canada, [3]Program in Atmospheric and Oceanic Sciences, Princeton University, Princeton, New Jersey, USA

Abstract Stick-slip behavior is a distinguishing characteristic of the flow of Whillans Ice Stream (Siple Coast, Antarctica). Distinct from stick slip on Northern Hemisphere glaciers, which is generally attributed to supraglacial melt, the behavior is thought be controlled by basal processes and by tidally induced stress. However, the connection between stick-slip behavior and flow of the ice stream on long time scales, if any, is not clear. To address this question we develop a new ice flow model capable of reproducing stick-slip cycles similar to ones observed on the Whillans Ice Plain. The model treats ice as a viscoelastic material and emulates the weakening and healing that are suggested to take place at the ice-till interface. The model results suggest the long-term ice stream flow that controls ice discharge to surrounding oceans is somewhat insensitive to certain aspects of stick-slip behavior, such as velocity magnitude during the slip phase and factors that regulate it (e.g., elastic modulus). Furthermore, it is found that factors controlling purely viscous flow, such as temperature, influence stick-slip contribution to long-term flow in much the same way. Additionally, we show that viscous ice deformation, traditionally disregarded in analysis of stick-slip behavior, has a strong effect on the timing of slip events and therefore should not be ignored in efforts to deduce bed properties from stick-slip observations.

1. Introduction

Stick-slip behavior of glaciers and ice streams continues to be a puzzling feature of land ice dynamics. Though the behavior is observed on outlet glaciers in both hemispheres [*Fischer and Clarke*, 1997; *Chandler et al.*, 2005; *Danesi et al.*, 2005; *Zoet et al.*, 2012], a particularly conspicuous and well-observed example is that of Whillans Ice Stream (formerly Ice Stream B)—and specifically the wide, flat region in the mouth of the stream known as Whillans Ice Plain [e.g., *Bindschadler et al.*, 2003; *Winberry et al.*, 2009, 2011]. A characteristic pattern of stick-slip behavior is prolonged stagnation (the "stick" phase) interrupted by short bursts of movement (the "slip" phase) approximately twice a day [e.g., *Bindschadler et al.*, 2003; *Winberry et al.*, 2009]. Stick-slip is not limited to glaciers; it occurs in various geophysical contexts and has been proposed as a mechanism for certain types of earthquakes [*Brace and Byerlee*, 1966]. Thus, analyses in a glaciological context rely heavily on approaches used in other fields [e.g., *Wiens et al.*, 2008; *Walter et al.*, 2011].

It is not entirely clear what controls the stick-slip dynamics of Whillans Ice Plain. In the Northern Hemisphere, the oscillations are thought to be forced by diurnal variations in basal water pressure [e.g., *Fischer and Clarke*, 1997]. However, on the Siple Coast Ice Streams there is not enough surface melt to supply water to the bed and influence its dynamics. It is thought that the periodic acceleration is triggered by plastic failure of the underlying till, caused by buildup of elastic stresses in the ice, and regulated by ocean tidal height at the downstream end of the ice plain (which has an effect on stresses within the ice) [*Bindschadler et al.*, 2003]. Not much is known, however, about the basal environment underlying the stream. It has been proposed that a rate-weakening mechanism is required for stick-slip motion to be favored over steady sliding [*Winberry et al.*, 2009; *Sergienko et al.*, 2009], which is in contrast with lab studies on Whillans Ice Stream till samples that do not indicate any strong dependence of shear strength on velocity [*Tulaczyk et al.*, 2000; *Iverson*, 2010].

Stick-slip motion is interesting in and of itself, since it exhibits dynamics that are highly nonlinear and operates on time scales much shorter than previously thought important for Antarctic ice streams. The

phenomenon has farther-reaching implications, however. Its observations have the potential to provide information about the complicated basal processes guiding them—information that is currently lacking due to the difficulty in sampling the ice-bed interface, and the apparent disconnect between lab- and large-scale behavior [*Winberry et al.*, 2009].

From the perspective of large-scale ice dynamics, the relevant aspect of stick-slip motion is its contribution to velocities over longer time scales (i.e., years to decades). It is important to realize that slip events are not merely perturbations around the mean flow of Whillans Ice Plain; rather, in areas where stick slip is known to occur, slip events comprise the bulk of total horizontal motion. This can be seen by considering the scale of typical slip displacements (30–40 cm) and recurrence periods (8–17 h) [*Bindschadler et al.*, 2003; *Winberry et al.*, 2009], giving average velocities of ∼150–420 m/a, which is on the order of velocities measured through remote sensing [*Joughin et al.*, 2002]. Therefore, stick slip represents a distinct mode of flow, one for which the ice dynamics are not as well understood as those addressed in more conventional glacial flow studies. Given the uncertainty of the rate-weakening mechanism under Whillans Ice Stream, it cannot be ruled out that other ice streams have the potential to exhibit stick-slip behavior, even though they do not currently. It has been suggested that observed stick slip is related to a slow deceleration of the ice stream [*Joughin et al.*, 2005; *Sergienko et al.*, 2009]. Moreover other Siple Coast streams have undergone similar deceleration in recent millennia [*Hulbe and Fahnestock*, 2004; *Catania et al.*, 2012], though it is not known whether these streams would have exhibited stick-slip behavior. Thus, it is important to understand the dynamics of stick-slip motion, both for what it can tell us about the subglacial environment and for its potential contribution to large-scale flow.

The goals of this study are to investigate ice stream stick-slip behavior using a modeling framework which can connect short- and long-time scale behavior and to investigate the controls that various factors have on each. Our modeling approach to stick slip is novel in that we account for both reversible and irreversible ice deformation, connecting short-term stick-slip behavior with longer-term ice flow. Also, we use a rate-weakening sliding law that is suitable for a glaciological flow model. The model is applied to an idealized geometry with scales and properties similar to those of Whillans Ice Plain. This allows for investigation of the effects of transverse variability, so far disregarded in previous studies.

The paper is structured as follows: in section 2 we present the equations of the continuum model used in this study, including the parameterization used for friction at the ice-bed interface. In section 3 we demonstrate the model's ability to exhibit slip events and begin to explore the connection with time-averaged flow. In section 4 we investigate the role of ice viscosity in the stick-slip cycle, particularly in the timing of slip events and how this relates to average flow. Section 5 explores the implications of the prior section's results for inferring bed properties from stick-slip observations. Finally, in section 6, we then investigate the role of tidal forcing in the model.

2. Continuum Model of an Ice Stream

Most up-to-date studies employ some form of block-and-slider model that approximates ice deformation as elastic [e.g., *Bindschadler et al.*, 2003; *Sergienko et al.*, 2009; *Winberry et al.*, 2009; *Walter et al.*, 2011]. However, glacial ice is known to deform both plastically and elastically [*Jellinek and Brill*, 1956]; thus, elastic models are not capable of capturing long-term flow characteristics. On the other hand, glaciological models that are meant to capture the long-term evolution of ice (on the scale of decades or longer) ignore the elastic components of its rheology.

A decisive factor that determines the appropriate treatment (viscous or elastic) is the Deborah number, De, a ratio of T_M, the Maxwell time, to the time scale of a phenomenon. T_M is the ratio of viscosity to elastic modulus; on time scales shorter than T_M a viscoelastic material such as ice behaves elastically, and on longer time scales it can be considered viscous [*Maxwell*, 1867]. Thus, a large De implies an elastic treatment. The characteristic value for ice viscosity is $\sim 10^{14}$–10^{16} Pa s (depending on effective strain rate), and ∼10 GPa for Young's modulus, giving Maxwell times ranging anywhere from half a day to several months. Thus, during slip events that last 10–30 min ice deformation is clearly elastic ($De \gg 1$). On the other hand, during stick phases that last from several hours up to a day, ice deformation might be viscous ($De \lesssim 1$).

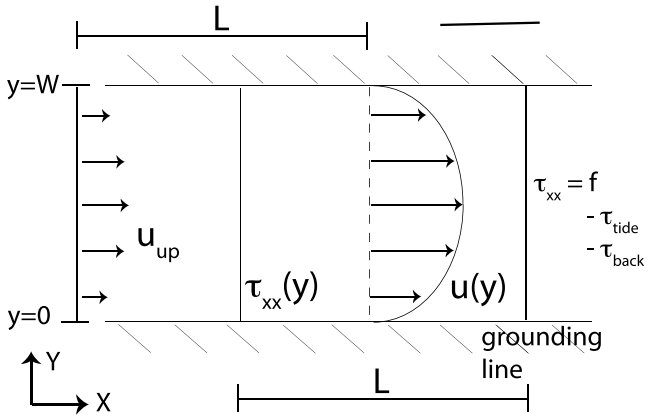

Figure 1. Top-down (plan) schematic of ice stream model. $u(y)$ is seaward velocity at a distance $L/2$ upstream from the front, and $\tau_{xx}(y)$, the calculated longitudinal stress, is considered a distance $L/2$ upstream from modeled velocity.

To account for both modes of ice deformation (viscous and elastic), we use a nonlinear Maxwell rheology; while linearly elastic, the rheology incorporates the non-Newtonian viscous behavior (Glen's flow law) exhibited by glacial ice on longer time scales. A Maxwell material represents the simplest possible rheology that allows for both viscous and elastic deformation, though other types of viscoelastic rheology (e.g., Burgers) have been used to explain tidal bending of ice shelves [*Reeh et al.*, 2003] and tidal modulations of ice streams [*Gudmundsson*, 2011]. Further, ice is assumed incompressible; this assumption is discussed below.

In our flow model, the domain is assumed to be bounded laterally by rigid sidewalls (Figure 1), with a specified upstream velocity profile (described below). At the grounding line, longitudinal stress is set by a hydrostatic pressure imbalance between ice and ocean, minus an ice shelf backstress (i.e., the cumulative effect of ice shelf buttressing, which can be substantial in Antarctic ice shelves). The model is noninertial, as is common for glacial flow models, and justified in this case by consideration of acceleration scales as recorded by GPS observations (there are faster, more transient accelerations associated with seismic waves and rupture propagation [*Pratt et al.*, 2014]). Further, stresses are hydrostatic and velocities are depth independent, which is suitable for ice sliding over weak beds [e.g., *MacAyeal*, 1989]. Through the grounding line stress, tidal forcing can be implemented by changing ocean height. The driving stress term $\rho g H \nabla H$ is assumed negligible relative to the effect of the grounding line stress, representing the relatively low driving stresses on Whillans Ice Plain [*Joughin et al.*, 2004].

To reduce computational expense, we (a) assume that transverse movement (i.e., flow in the y direction) is negligible, or otherwise unimportant to leading-order behavior, and (b) parameterize along-flow variations. The latter is done by approximating along-flow gradients as $\partial_x(\cdot) \approx \frac{(\cdot)}{L}$ (where L is a specified length scale). These two procedures simplify the model somewhat but still allow us to resolve the effect of lateral shear, a factor that has been disregarded in previous studies.

The stress balance (in the x direction) is given as

$$-\frac{2}{L}\tau_{xx} + \frac{1}{H}\partial_y(H\tau_{xy}) - \frac{\tau_b}{H} = -\frac{2}{L}\tau_{\text{front}}, \tag{1}$$

$$\tau_{\text{front}} = \frac{1}{H}\left[\frac{1}{2}\rho_i g H^2 - \frac{1}{2}\rho_w g\left(\frac{\rho_i}{\rho_w}H + \eta_{\text{tide}}\right)^2\right] - C_b\tau_{\text{unc}}. \tag{2}$$

Here $\rho_{i,w}$ are densities of ice and water, respectively, and τ_{front} is imposed longitudinal stress at the grounding line. τ_{unc} is equal to $\frac{1}{2}\rho_i\left(1-\frac{\rho_i}{\rho_w}\right)H$, the stress when the ice shelf is unconfined (or nonexistent). C_b is a parameter between 0 and 1, which specifies the level of buttressing ($C_b = 1$ is the completely buttressed case, meaning driving stress is minimal). The effect of tides on normal stresses in the ice is introduced through τ_{front}. The expression within brackets in equation (2) is the difference of depth-averaged hydrostatic pressure on the grounded and floating (or ice free) sides of the grounding line. The term within parentheses represents the ocean column depth at the grounding line, equal to the floatation depth in the absence of tidal fluctuations—which are represented by η_{tide}. Note that when $\eta_{\text{tide}} = 0$, the term in brackets is equal to τ_{unc}.

The constitutive relation used for ice is one of a Maxwell material with linear elasticity and Glen's law viscosity [*Gudmundsson*, 2011]:

$$\dot{\tau}_{xx} = 2Gu_x - \frac{G}{\nu}\tau_{xx} + \epsilon\mathcal{N}_{xx}, \tag{3}$$

$$\dot{\tau}_{xy} = Gu_y - \frac{G}{\nu}\tau_{xy} + \epsilon\mathcal{N}_{xy}, \tag{4}$$

$$\nu = \frac{1}{2A(\theta)}\left(\tau_{xx}^2 + \tau_{xy}^2 + \varepsilon_\tau^2\right)^{\frac{1-n_g}{2}}, \tag{5}$$

$$\mathcal{N}_{xx} = -u\partial_x\tau_{xx} + 2\tau_{xx}u_x,$$

$$\mathcal{N}_{xy} = u_x\tau_{xy} + \frac{1}{2}\tau_{xx}u_y.$$

Here n_g is Glen's flow law exponent (equal to 3 here), G is the shear modulus, and A is a temperature-(θ-)dependent scalar that causes the ice to soften as it warms [*Paterson*, 2001]. In this model, temperature is a specified parameter, and taken to be a depth-averaged temperature—a proxy for thermodynamic state of an ice stream. ε_τ is a regularization parameter, equal to 10^{-2} Pa. Note that due to the non-Newtonian rheology, viscosity is not spatially constant but instead increases as stress decreases. The terms denoted by $\mathcal{N}_{ij}$ are advective and codeformational (i.e., associated with a deforming coordinate frame) terms; they are expected to be small. A parameter ϵ, set to either 1 or 0, controls whether terms $\mathcal{N}_{ij}$ are accounted for or disregarded. Similar to the divergence of τ_{xx}, u_x is parameterized as

$$u_x \approx \frac{u - u_{\text{up}}}{L}, \tag{6}$$

where u_{up} is an imposed upstream velocity profile, chosen as that of an ice stream with no motion at its lateral boundaries, in which horizontal shear stress balances a constant driving stress:

$$u_{\text{up}}(y) = \frac{5u_*}{4}\left(1 - \left(1 - \frac{2y}{W}\right)^4\right). \tag{7}$$

The parameter u_* sets the mean upstream velocity. Lastly, we are concerned with time scales germane to one or several slip events, and over these, ice thicknesses change negligibly. Hence, we treat ice thickness H as both spatially uniform and constant in time.

Note that by disregarding the inertia terms we eliminate the propagation of elastic waves. This is justified by the fact that in ice these wave speeds are ~3 km s^{-1} for *p* waves and ~1.5 km s^{-1} for *s* waves [*Kirchner and Bentley*, 1979]. These waves propagate through the entire ice plain in 7–15 s, which is much faster than the duration of a event (~15–30 min) [*Wiens et al.*, 2008]. We note that slower-moving elastic waves within the till or along the ice-till interface, with average speeds of ~150 m/s, have been suggested as mechanisms of slip propagation [*Bindschadler et al.*, 2003], though recent work suggests rupture front propagation up to ~1 km/s immediately after nucleation [*Pratt et al.*, 2014].

Our assumption of incompressibility is fairly common when considering purely viscous ice deformation, although estimates of parameters relating to elastic deformation imply compressibility [*Schulson*, 1999]. However, previous studies of viscoelastic ice stream flow have implicitly considered ice to be incompressible or near-incompressible [e.g., *Gudmundsson*, 2011; *Walker et al.*, 2012]. While this assumption would certainly impact elastic wave solutions, we do not attempt to resolve such phenomena, as mentioned above.

Our assumption of negligible transverse flow is made on the basis that the ice stream is laterally confined and the applied forcing is entirely in the along-flow direction. It is heuristic, and its veracity can only be assessed with a model that resolves both horizontal directions, such as that of *Rosier et al.* [2014]. A compressible rheology and the use of a two-dimensional model are intended directions of future investigation. We also assume that the ice stream is in hydrostatic equilibrium and do not resolve any tidally induced flexure. Similarly, this is deferred for the future studies.

2.1. Rate-Weakening Base

Several studies have suggested that glacial stick-slip oscillations owe their existence to the complexity of the physics of basal sliding [e.g., *Fischer and Clarke*, 1997; *Bindschadler et al.*, 2003; *Winberry et al.*, 2009; *Sergienko et al.*, 2009; *Walter et al.*, 2011; *Zoet et al.*, 2012]. Many authors argue that some sort of rate-weakening is

Table 1. Parameters in Continuum Model

Parameter Name	Description	Value
H	ice stream thickness	750 m
L	along-flow length scale	80 km
W	ice stream width	100 km
G	ice elastic modulus	10^{10} Pa
u_*	upstream ice velocity	variable
C_b	degree of buttressing at grounding line	variable (0 to 1)
ρ_i	ice density	917 kg m^{-3}
ρ_w	ocean density	1028 kg m^{-3}
θ	ice temperature	variable
A	Glen's Law flow constant	function of θ
n	Glen's Law exponent	3
ϵ	"switch" for advective and codeformational terms	0 or 1
τ_s	upper limit of yield stress	variable
τ_k	lower limit of yield stress	variable
T_b	yield stress time constant	0.1 h
u_0	velocity transition scale for yield stress	250 m/yr
ϵ_τ	minimum internal stress	0.01 Pa
u_ϵ	plastic bed rheology regularization parameter	1 m/yr

required, where basal stress is lower during the slip phase than during the stick phase; but the details, and the mechanism, of such weakening are not known (see *Iverson* [2010] for an insightful discussion on this topic). Here no attempt is made to represent the detailed physics of the till and hydrological system underlying the ice stream. Instead, a very simple phenomenological approach is adopted, in order to capture the velocity-weakening property that has been proposed for the basal till under Whillans Ice Stream. The bed responds to shear stress with a plastic rheology, a commonly used basal stress model for Siple Coast ice streams [e.g., *Joughin et al.*, 2004]. Additionally, the yield stress τ_{yld} evolves locally depending on velocity:

$$\begin{aligned} \dot{\tau}_{\text{yld}} &= \frac{1}{T_b}\left(\tau_{\text{ss}} - \tau_{\text{yld}}\right), \\ \tau_{\text{ss}}(u) &= \tau_k + (\tau_s - \tau_k)e^{-\frac{|u|}{u_0}}. \end{aligned} \tag{8}$$

In other words, yield stress relaxes (with time constant T_b) to a sliding velocity-dependent steady state yield stress, τ_{ss}. As long as $\tau_k < \tau_s$, this is a rate-weakening formulation. These parameters, as well as T_b and u_0, are chosen based on order-of-magnitude estimates, and their influence is investigated in section 3.

We point out that equation (8) is heuristic and to our knowledge has not previously been used for this problem. However, the expression has some elements in common with rate-and-state laws [*Dieterich*, 1978; *Ruina*, 1983], which have been used to study friction in rock faults and sediments [*Rathbun et al.*, 2008]. In particular, it can be shown that our basal friction parameterization is very closely related with a "slip"-type rate-and-state law [*Rubin and Ampuero*, 2005]; we show this in detail in the supporting information. Given the uncertainty of the mechanism, we choose to use this phenomenologically based treatment. We point out, however, that our model is also capable of accommodating more commonly used forms of rate-and-state friction; experiments are presented in the supporting information.

To avoid numerical difficulties associated with a plastic bed, we use a regularized formulation:

$$\tau_b^{\epsilon}(u) = \tau_{\text{yld}}\frac{u}{\sqrt{u^2 + u_\epsilon^2}}. \tag{9}$$

Similar approaches have been used to represent purely viscous ice sliding over a plastic bed [e.g., *Bueler and Brown*, 2009; *Martin et al.*, 2010].

The model parameters are summarized in Table 1 and have the values stated there unless otherwise indicated. Numerical implementation is described in Appendix A.

2.2. The Stick-Slip Mechanism

In most of our experiments with the model, one of two extremes is considered with respect to external forcing. In one, $C_b < 1$ and $u_* = 0$; that is, the momentum balance is dominated by gravitational driving

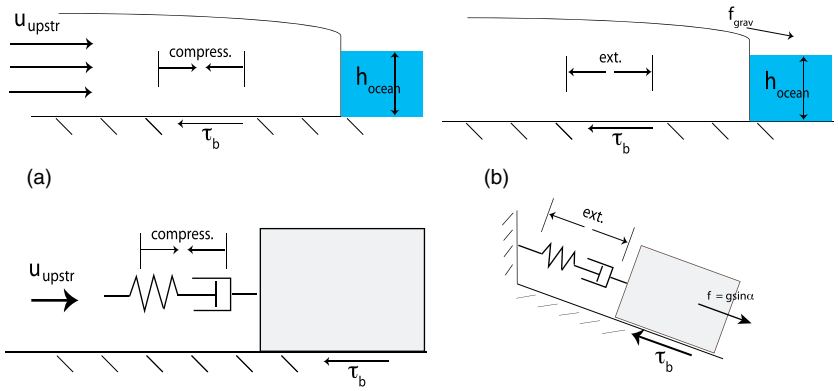

Figure 2. (a) Stick slip driven by pushing from steadily sliding ice upstream. The bed is loaded due to compression, and slip occurs when the bed yields, not unlike the block-slider models used in laboratory and conceptual studies (below). In this slider model, the spring is in series with a dashpot to allow for irreversible deformation. (b) Stick slip driven by gravitational driving stress. In this case stress due to extension (and lateral shearing) takes some of the burden from the bed. When the stress dissipates basal stress increases and the bed yields. This situation is analogous to a block-slider model on an inclined plane (below).

stress. We refer to this extreme below as a "stress-driven" experiment. In the other, $C_b = 1$ and $u_* > 0$—the momentum balance is dominated by upstream velocity. We refer to this as a "push-driven" experiment. Our goal is to examine stick-slip behavior when one of the two driving mechanisms is dominant and how model parameters (e.g., temperature) affect the behavior in each case.

The general process by which stick slip occurs can be easily described in each case. In the push-driven model, the upstream velocity compresses the stream longitudinally, leading to a positive longitudinal stress divergence that must be balanced by basal stress. Eventually, basal stress reaches the (static) yield stress and the ice plain begins to move. This in turn rapidly weakens the bed, and the resulting force imbalance leads to a slip event. During slip, the high velocities and associated buildup of elastic strain result in increased resistive shear and less compressive (or possibly extensive) longitudinal stress, slowing the ice plain. Eventually, the movement ceases and the bed strengthens again. The rapid weakening and strengthening of the bed is expected to play an necessary role.

This process can be seen as analogous to the block-and-slider models used in previous studies of stick slip, in which a block sits on a frictional surface, acted on by an external velocity through an elastic spring [*Bindschadler et al.*, 2003; *Sergienko et al.*, 2009; *Winberry et al.*, 2009]. A more complete analogy would replace the spring by a spring in series with a dashpot, a common conceptual model for a Maxwell material, to reflect the rheology of the ice stream (Figure 2a). In this block-and-slider model the dashpot component allows for some irreversible deformation, as opposed to the purely elastic slider.

In the stress-driven model, the mechanism is slightly different: the shear and longitudinal stress work together with the basal stress in resisting the gravitational driving stress. In this case, following a slip event, internal stresses are sufficiently large that the bed does not yield. However, viscous dissipation in the ice decreases the internal stress, effectively increasing load on the bed, to the point where the bed yields, and a slip event occurs. As in push-driven slip, this leads to a buildup of elastic stress which slows the ice. An appropriate block-and-slider analogue for this mechanism is one in which the block is on an inclined plane and anchored by the spring-and-dashpot apparatus (Figure 2b). An important point is that in this case, viscous dissipation is an integral part of the stick-slip mechanism (whereas only elasticity and rate-weakening friction are required for the push-driven mechanism).

3. Model Behavior

In this section we examine the behavior exhibited by the model, and its dependence on various parameters. Tidal forcing is excluded (tides are considered in section 6). We begin by simulating stick slip in the two regimes, stress driven and push driven. In these experiments, τ_s and τ_k are 3 kPa and 2 kPa, respectively, and $T_b = 0.1$ h. These parameters reflect order-of-magnitude estimates of basal stress, drop in basal stress

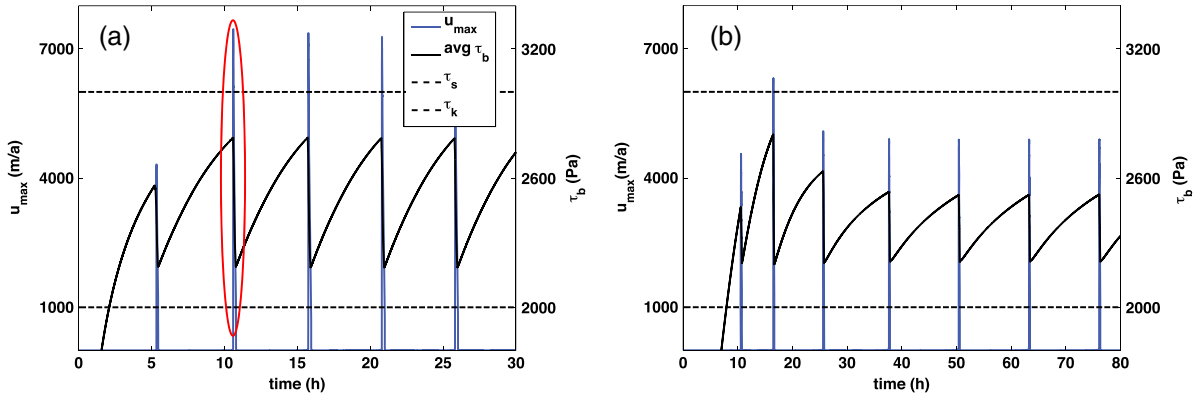

Figure 3. Time series for stick-slip simulations. (a) Stress-driven experiment. Maximum velocity of profile (blue) is plotted over time, as is averaged basal stress (black). Dotted lines show τ_s and τ_k from equation (8). (b) Push-driven experiment.

during a slip event, and slip duration for Whillans Ice Plain. Other parameters are as follows: ice thickness is 750 m, stream width is 100 km, length scale L is 80 km, the time step is 10^{-3} h (3.6 s), and the grid resolution is 1 km. The parameter ϵ is zero; however, setting it to 1 (i.e., allowing codeformational and advective terms) reveals almost no change in the results (not shown), and subsequently the terms $\mathcal{N}_{ij}$ are disregarded.

In the stress-driven experiment, $C_b = 0.5$, $u_* = 0$, and $\theta = -15°$C. The initial conditions for all fields are zero, except for shear stress, which is initialized such that it balances the gradient imposed by τ_{front}. Figure 3a summarizes the results. It shows maximum velocity (u_{max}) and width-averaged basal stress ($\overline{\tau}_b$) over time. That is,

$$u_{\text{max}}(t) \equiv \max_{0<y<W} u(y,t) \quad \text{and} \quad \overline{\tau}_b(t) \equiv \frac{1}{W}\int_0^W \tau_b(y,t)\text{d}y.$$

Intermittent peaks in u_{max} shown in Figure 3 represent slip events. In between slip events, basal stress increases; during the slip event, it drops again. The system appears periodic even though all forcings are constant in time. Note $\overline{\tau}_b$ does not attain its limits, τ_k and τ_s, although these values are attained at certain locations.

In the push-driven experiment (Figure 3b), $C_b = 1$, $u_* = 500$ m/a, and $\theta = -27.5°$C. (As shown in the next section, purely push-driven stick slip does not necessarily occur if temperatures are warm enough, i.e., if ice is "soft" enough.) Initially, slip events are more erratic than in the stress-driven case, but a limiting cycle is eventually realized. During the stick-slip cycles, the lower bound of $\overline{\tau}_b$ is close to that of the stress-driven experiment, indicating similar bed conditions during the slip events—but the upper bound is much lower. The difference reflects a different pattern of yield stress at the onset of slip: in the stress-driven case, a greater portion of the bed is yielded (or close to yielding). Aside from this distinction, however, slip event characteristics are very similar between the push- and stress-driven models, and so in the remainder of the section we focus primarily on the latter.

Figure 4 shows one of the slip events from the stress-driven experiment (denoted by a red ellipse in Figure 3a) in greater detail. Maximum velocity (Figure 4a) is asymmetric during the slip event. Aside from an abrupt shutdown at the end, the decelerating branch can be approximated to a good degree by an exponential function $\propto e^{-\frac{t}{T}}$, with $T \sim 0.1$ h. This is not a coincidence: rather it demonstrates that the relaxation time constant T_b in expression (8) determines the time scale of the slip event.

Figure 4b shows instantaneous velocity profiles at discrete times after the peak velocity of the slip event. During the slip event shear strain rates are considerable due to the no-slip conditions at the lateral boundaries. This causes a rapid increase in resistive shear stress due to elasticity. The increased shear stress, and a similarly increased longitudinal stress, slow the ice stream. During much of the deceleration, yield stress is in the "weak" state over a large part of the ice stream. Eventually, near the end of the slip event, velocity is small enough for basal stress to transition. Some parts of the bed strengthen before others, and this marks the rapid shutdown at the end of the slip event. Prior to this rapid shutdown (~10.5 min into the slip event), the velocity profiles appear to be self-similar. Examining the last two profiles, the shutdown

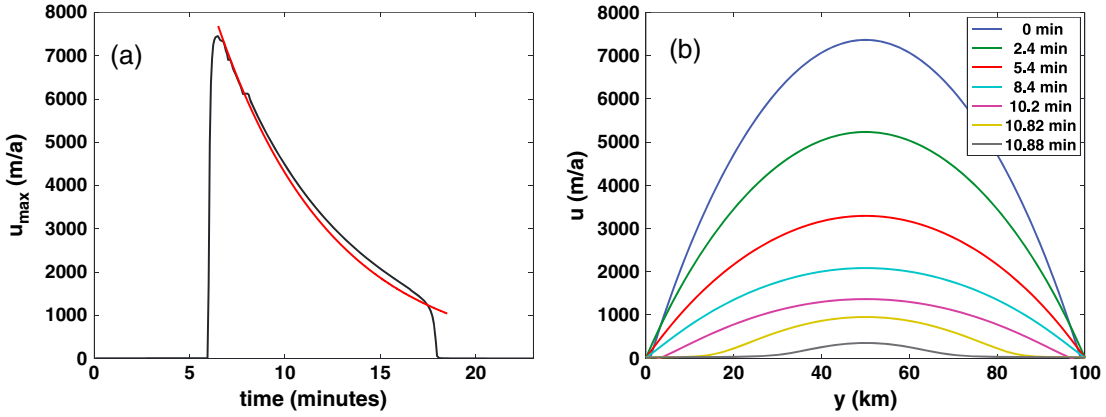

Figure 4. (a) Closer look at the slip event circled in Figure 3. The red curve is an exponential with decay constant T_b = 0.1 h. (b) Instantaneous velocity profiles during the slip event. The labels indicate elapsed time since that of peak velocity.

appears to travel rapidly inward from the margins. Note the self-similarity of the velocity profiles, prior to the rapid shutdown.

In the model, slip onset is essentially instantaneous. (From Figure 4a, slip onset may appear to occur over a finite time scale, but this is due to a small regularizing inertial damping term; see Appendix A for details.) It is likely that slip onset is regulated by processes that are not resolved by our model, such as seismic waves within the till or at the ice-till interface. Recent work [*Winberry et al.*, 2011; *Pratt et al.*, 2014] suggests that the onset of slip is extremely complex and heterogeneous, with multiple points of nucleation and rupture front speeds that vary from ~100 m/s to over 1 km/s. The homogeneity of basal parameters and parameterization of the along-flow dimension in our model prevents us from fully exploring this complexity. We remark, however, that slip onset not always instantaneous in our model, e.g., if the bed parameters are allowed to vary spatially (not shown). Thus, it may be possible to capture some aspects of slip onset, even though we do not resolve seismic wave propagation.

On the other hand, the shutdown does not appear to be discontinuous in our model; further experiments suggest that the speed with which shutdown occurs, though rapid, is limited as time step is decreased, suggesting our model might capable of capturing the slip shutdown process. In any event, both slip onset and shutdown have a relatively small effect on the maximum slip velocity, the duration of the stick and slip phases, and the time-averaged velocity due to stick slip.

It is interesting to consider how the parameters governing the time-dependent behavior of basal stress—T_b and u_0—affect the slip event. In Figure 5a, it can be seen that when T_b, the bed transition time scale, is doubled from 0.1 to 0.2 h, the maximum slip velocity is approximately halved, and the slip event is longer (though less than twice as long). Again, throughout most of the slip event, u_{max} agrees well with an exponential decay function, in this case with a rate of 0.2 h. When u_0, the parameter determining the shape of $\tau_{ss}(u)$, is doubled from 250 m/a to 500 m/a, the maximum velocity profile is nearly identical to that of the original experiment throughout most of the event, although it terminates slightly earlier. T_b and u_0 also have an effect on the duration of the stick phase, but the effect is small, on the order of minutes. (The slip events in Figure 5a have been shifted, so their onsets coincide.) If T_b is large ($\gtrsim$ 1 h) or $\tau_s \leq \tau_k$ (not shown), stick-slip cycling does not occur. Thus, rapid weakening of the bed in response to speedup (and healing in response to deceleration) is a necessary component of the process.

We also consider how these changes to the slip events affect time-averaged velocity. Figure 5b shows profiles of $\overline{u}(y)$—the time-averaged velocity—corresponding to the experiments in Figure 5a. We define $\overline{u}$ as

$$\overline{u}(y) = \frac{1}{(t_2 - t_1)} \int_{t_2}^{t_2} u(y,t)\mathrm{d}t, \tag{10}$$

where t_1 and t_2 are the times of consecutive slip events; that is, $t_2 - t_1$ is the stick-slip period. As the contribution of stick-slip motion to the long-term evolution of the ice plain, time-averaged velocity is perhaps more important from a glaciological perspective than other details of the stick-slip cycle, such as maximum

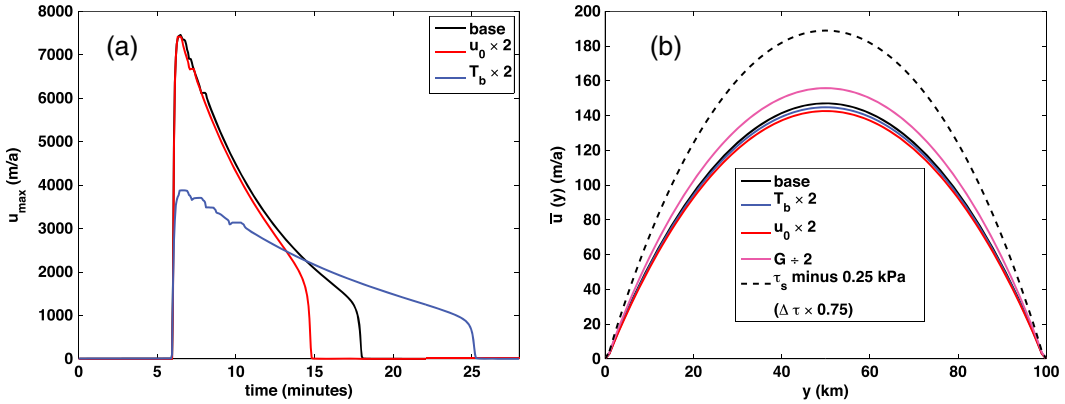

Figure 5. (a) Sensitivity of (maximum velocity of) slip event to parameters. Profiles are shifted so that slip onsets are coincident. (b) Sensitivity of time-averaged velocity ($\bar{u}$) to parameters.

velocity or slip frequency. Interestingly, u_0 and T_b have almost no effect on $\bar{u}$. The Young's modulus G is also modified: dividing G in half has the effect of approximately doubling the interslip duration, but it has very little effect on the average velocity. It seems these controls on slip behavior, and frequency are negligible on time scales of days or longer. Bed strength does have a strong control on average velocity, however. Decreasing the stress drop $\tau_s - \tau_k$ by 25% (by decreasing τ_s) increases $\bar{u}$ by a comparable amount. Ice viscosity is an important control on time-averaged velocity as well; this is investigated in detail in the following section.

To get insights in fundamental aspects of the model, we have considered a simplified version that has linear ($n = 1$) viscosity. Such a model can be treated analytically. Its asymptotic solution predicts many aspects of the stick-slip solution, including the instantaneous slip onset, the self-similar velocity profile and its exponential decay during the slip events, and the (in)dependence of time-averaged flow on T_b, u_0, and G. The asymptotic solution also provides scalings for maximum velocity and duration of slip events. Moreover, the solution provides numerical validation: the numerical model was adapted to solve the simplified equations, and excellent agreement between numerical and asymptotic solutions was observed. We present the solution and validation experiments, in the supporting information.

It should be emphasized that the behavior of the model is also strongly influenced by its "geometric" parameters: ice stream thickness, width, and length. For instance, a decrease in the length scale would increase the role of longitudinal stress in the force balance and lead to a shorter stick-slip period for either push- or stress-driven experiments. These types of dependencies are considered in previous modeling studies [e.g., *Winberry et al.*, 2009; *Sergienko et al.*, 2009; *Walter et al.*, 2011]. However, the influence of viscosity on stick-slip behavior has not been investigated.

4. The Role of Viscosity

Given a high Deborah number, we do not expect viscous effects to play a role in slip events; however, they could be important on the time scale of stick intervals. Viscosity is not controlled directly in the model but is variable and dependent on the local stress terms, and the scale of the viscosity depends on the Glen's law constant A, which has a known dependence on temperature [*Paterson*, 2001]. All else held constant, the warmer the ice, the less viscous. Here we use this property to phrase our discussion on the effect of viscosity in terms of ice temperature, though there could be other factors (e.g., solute content, fracture density) that could conceivably alter viscosity in the same way.

Figure 6a shows the effect of temperature on stick-slip in a stress-driven model. The chosen parameters are the same as for Figure 3a, except for temperature, which takes on values −16°C (red) and −21°C (blue). In the warmer (less viscous) case, the stick-slip period is about 6 h, while in the colder (more viscous) case it is about 10 h. Shown as well are cumulative movement of the center of the ice stream in the two cases. As anticipated, the slip distances are roughly equivalent, but due to the differing stick interval durations the average velocities are very different (Figure 6b).

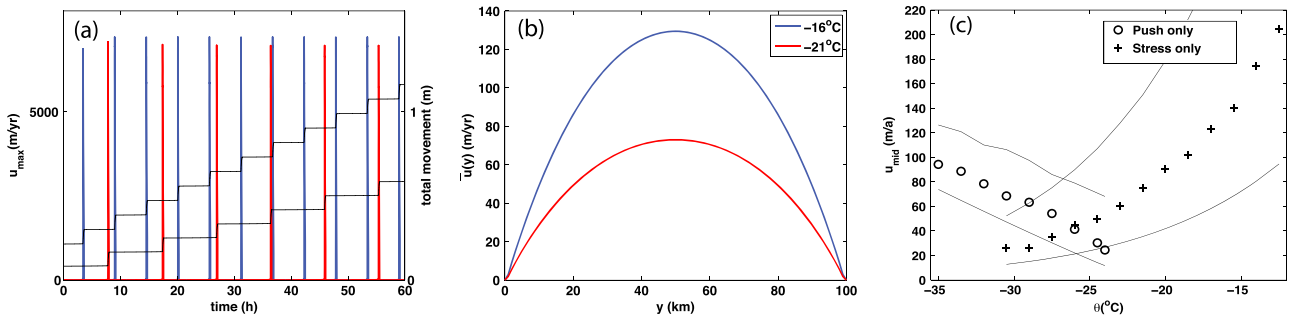

Figure 6. Response to varying temperature, no tidal forcing. (a) Maximum velocity, $\theta = -16°C$ (blue) and $-21°C$ (red). Black curves are corresponding cumulative displacement. Both simulations are stress-driven ($u_* = 0$). (b) Velocity profile averaged over a stick-slip cycle, corresponding to simulations in Figure 6a. (c) Time-averaged velocities at $y = W/2$ as a function of temperature, stress-driven and push-driven models. Solid lines indicate steady sliding velocities with $\tau_{yld} \equiv \tau_k$ or τ_s. For $\theta \gtrsim -24°C$, push-driven slip does not occur.

The dependence of average velocity on temperature (and hence viscous effects) is explored more fully in Figure 6c, where time-averaged velocity at the center of the stream is shown over a range of temperatures, for both the stress-driven and push-driven models. For a given model, the variations in average velocity are entirely due to variations in stick duration. Temperature is seen to affect the two models differently, with warmer temperatures (and hence softer ice) in the stress-driven model leading to more frequent slip events, and thus higher velocities, while softer ice in the push-driven model leads to sparser slip. For the push-driven model there is a temperature beyond which slip does not occur; in this case the elastic strain added by pushing is being dissipated so effectively that the stream is permanently "stuck." There is no such threshold in the stress-driven case; this is because of the differing stick-slip mechanisms. The critical temperature for slip in the push-driven model is not universal but depends on the upstream velocity and the geometric parameters of the model. Note that in the case of the stagnated stream, mass convergence would eventually modify driving stresses and drive motion; however, this would occur on time scales of years to decades, which are not considered here.

As mentioned in the previous section, viscosity is not the only factor determining slip timing. In the push-driven instance, if u_* were lowered, the duration of stick intervals would increase, and time-averaged velocity would slow, and there would be a threshold for u_*, dependent on other parameters, below which slip would not occur (not shown). This would lead to a shift in the flow behavior of the stream; however, since the stick interval durations become large as u_* is drawn down (and time-averaged velocity becomes small), the effect of this shift on time-averaged flow would be relatively minor.

Figure 6c also plots steady sliding velocities with yield stress constant in time and equal to either τ_s or τ_k. The time-averaged velocities do not coincide with either curve, but they do appear to have similar functional dependencies on temperature. In fact, similar behavior is seen with respect to other parameters, including ice stream width and driving stress (not shown): the response of time-averaged velocity is very similar to that of a purely viscous ice stream, only with an implied yield stress that lies somewhere between τ_s and τ_k.

5. Implications for Basal Stress Estimation

Observation of stick-slip behavior has the potential to yield information about the properties of the deforming bed—in particular, the point of failure and the magnitude of the weakening that takes place during a slip event (τ_s and $\tau_s - \tau_k$, respectively, in our bed model). However, it is the response of the ice that is directly observed, and this response must be deconvolved to make sense of basal properties. In *Winberry et al.* [2009], the timing of slip events was used to estimate total bed loading during the stick phase, which was in turn used to infer properties regarding bed strengthening. An assumption made in their study is that the ice response is elastic and hence that the bed loading rate (aside from the effect of tides) is constant.

We have shown that viscous effects in ice are likely to be important on the interslip time scale. So it is worth asking whether an elastic approximation is sufficient for assessing total stress loading, i.e., if viscous effects can be ignored. In the aforementioned study, the authors analyze a single time series with stick intervals

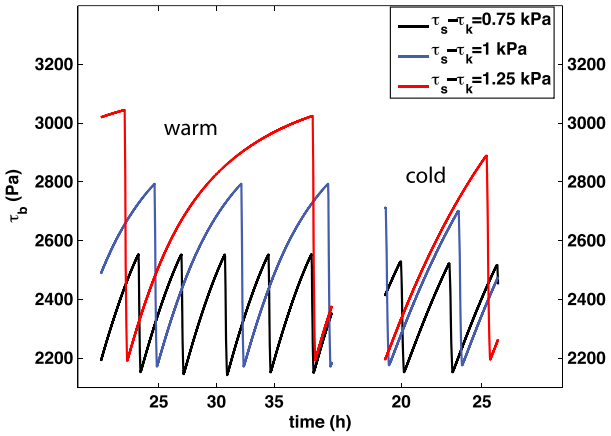

Figure 7. Average basal stress ($\overline{\tau}_b$) over time at (left) $\theta = -15°C$ and (right) $\theta = -30°C$. Different color curves correspond to different values of the parameter τ_s.

of varying lengths due to tides and other factors, from which they infer a slow strengthening of the bed in between slip events. We carry out a related experiment: we run multiple simulations, with differing "strong" bed states (i.e., differing values of τ_s) but identical weak bed states (τ_k), yielding differing stick phase intervals. By calculating and comparing average bed loading rates for these simulations, we can determine whether viscous effects should be taken into account to recover the stress drop ($\tau_s - \tau_k$). Specifically, if average loading rate is close to uniform with respect to τ_s, an elastic assumption may be sufficient.

Parameters are as in the experiments in Figure 6c, but with a length scale $L = 100$ km. We allow for both driving forces, gravitational driving stress and upstream pushing, with $C_b = 0.5$ and $u_* = 500$ m/a. Loading rates are determined by calculating the increase in average basal stress, $\Delta\overline{\tau}_b$, over the course of a stick interval, and dividing by the length of the interval:

$$\text{loading rate} = \frac{\Delta\overline{\tau}_b}{\Delta t_{\text{stick}}}. \tag{11}$$

Figure 7 shows the results of this exercise at two different temperatures, $\theta = -15°$C and $\theta = -30°$C. The values of τ_s are 2.75, 3, and 3.25 kPa, giving *local* stress drops of 0.75, 1, and 1.25 kPa, but as in earlier experiments, the average $\Delta\overline{\tau}_b$ is smaller. At the warmer temperature, effects of ice viscosity are more prevalent. Basal loading rates vary from ~52 to 114 Pa/h, depending on the length of the interval. Basal loading rate is more uniform at the colder temperature; however, over the same range of τ_s as in the warmer experiment, basal loading rates only vary from ~110 to 132 Pa/h.

Hence, whether the assumption of constant basal loading rate is appropriate for Whillans Ice Plain depends on its conditions. If a gradually decreasing loading rate is more realistic, as for the warmer case in Figure 7, then inferring basal loading from stick phase duration assuming a constant loading rate (as in *Winberry et al.* [2009]) would overestimate loading for longer intervals and therefore overestimate the amount of slow (hourly to daily) strengthening proposed.

The results of this section can be generalized through an approximated expression for the stick phase duration, derived in Appendix B. There we show that the degree of nonlinearity in basal stress loading is determined by the relative magnitudes of bed strength, τ_s, and a generalized driving stress scale

$$\alpha_N = 2HNE/L + F,$$

where N is a representative viscosity value, E is the compressive strain rate, and F is the driving stress. If $\alpha_N \gg \tau_s$ the stick phase duration scales with the stress drop ($\tau_s - \tau_k$), and the average loading rate is therefore uniform over a range of stress drops; otherwise, the average loading rate decreases as τ_s increases.

6. Effect of Tidal Forcing

Tides have been shown to play a role in the stick-slip process, with the period of the observed cycle matching that of tides [*Bindschadler et al.*, 2003; *Winberry et al.*, 2009, 2011]. Given that tidal forcing is always present [e.g., *MacAyeal*, 1984], it is academic for it to be ignored in an exploration of stick-slip behavior. However, in this section, we show that the unforced stick-slip period and the time-averaged velocity are robust properties of our model even in the presence of tidal forcing. The majority of the experiments in this section use the stress-driven model, as our implementation of driving stress through forcing at the ice front makes this the more natural setting; however, the push-driven model is examined as well.

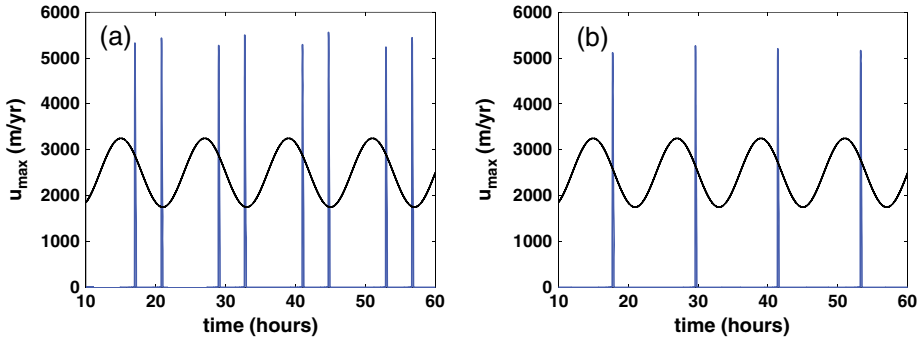

Figure 8. Maximum velocity with tidal forcing as given by equation (12), (a) $\theta = -16°C$ and (b) $-21°C$. Black curves show phase of tidal forcing. Both simulations are stress driven.

When tidal forcing is included, the results of the experiments from Figure 6a are modified, as shown in Figure 8. η_{tide} in equation (2) is given by

$$\eta_{\text{tide}}(t) = 1\,[\text{meter}] \cdot \sin\left(\frac{2\pi t}{12\,[\text{hours}]}\right), \tag{12}$$

where we have assumed an idealized 12 h tidal cycle with 1 m amplitude. The slip events appear to be closely correlated with the tidal forcing; however, while both experiments have a 12 h cycle, they exhibit different behavior. In the simulation with colder ice a single slip event per cycle occurs, while in the simulation with warmer ice a "doublet" structure appears, meaning a shorter stick phase interval is followed by a longer one.

We point out that our parameterization of tidal forcing (12) ties reduction in driving stress to tidal height. However, ice shelves respond viscoelastically to tides, and so the effect on driving stress is related to both bending displacement and bending rate of the shelf (R. Walker, personal communication, 2013). This is a possible explanation of why the first slip of a doublet in Figure 8a occurs some time after the peak in tidal height, while Figure 4 of *Winberry et al.* [2009] shows slip events immediately after the peak. The important point, though, is the degree to which ice viscosity (through temperature effects) controls the details of the cycle.

Figure 9 shows the time between successive slip events (the stick interval) as a function of slip event count for the two tidally forced experiments, as well as a third where $\theta = -18°C$. For this temperature we observe a complex 36 h cycle that is composed of both short (4–5 h) and long (8–11 h) length stick intervals. Thus, while the tidal period influences the length of the stick-slip cycle, the structure of the cycle is clearly influenced by the unforced periodicity.

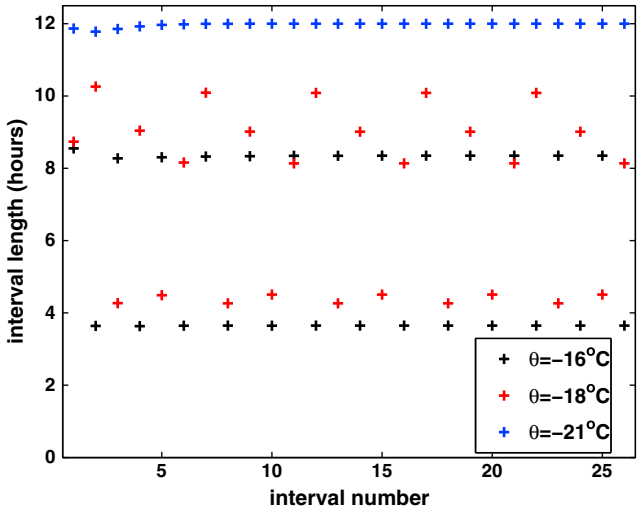

Figure 9. Progression of interval length for $\theta = -16°C$, $-18°C$, and $-21°C$ with 12 h sinusoidally varying tidal height. For $-16°C$ and $-21°C$, there is a 12 h period, with a "doublet" structure for $-16°C$, but for $-18°C$ there is a longer cycle. All simulations are stress driven.

The effect of the unforced frequency on the stick slip cycle be examined more concretely in the frequency domain. Figure 10 shows three different spectra, derived from the discrete Fourier transforms of u_{max}. To remove the effects of initialization from the time series, the model was run for 1000 h and only the last 750 h were examined. In one of the time series, $\eta_{tide} = 0$ (i.e., it is unforced). In another, $\eta_{tide} = 0.1$ m; this is in order to examine the weakly forced case. In a third, $\eta_{tide} = 1.0$ m, as in the experiments discussed above. In all

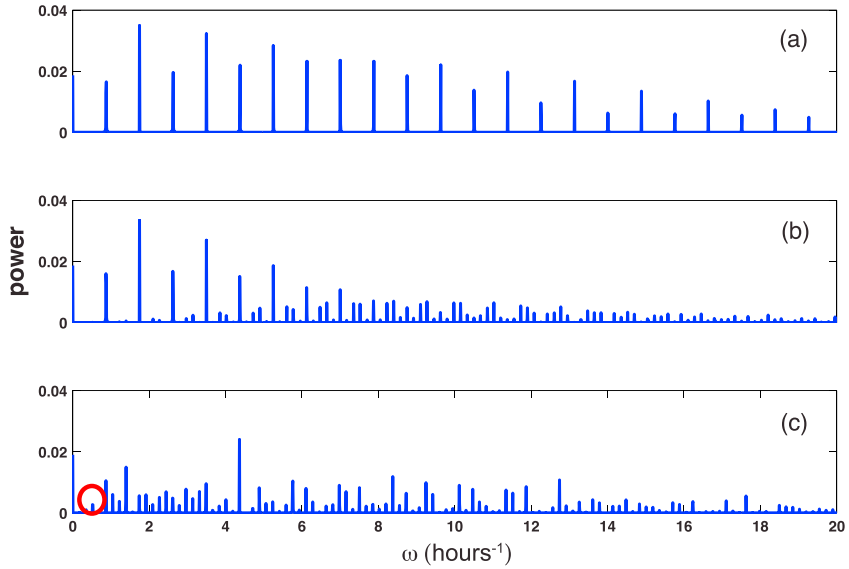

Figure 10. Spectra of time series of $u(y = W/2)$. η_{tide} = (a) 0 m, (b) 0.1 m, (c) 1 m. Temperature is −18°, and all other parameters are as in Figure 8.

experiments, $\theta = -18°$. The unforced spectrum shows a sequence of peaks evenly spaced at ~0.88 h^{-1}, or $\frac{2\pi}{T_n}$, where T_n is the unforced period of oscillation, with slow decay. This is typical for periodic functions approximating Dirac δ functions. The first peak corresponds to the slowest mode, i.e., the slip frequency. In the weak forcing case, the pattern from the unforced spectrum can still be seen quite clearly, almost superimposed with more closely spaced higher harmonics. At the low-frequency end, the spectrum is barely affected by the forcing. The 12 h tidal mode is present, but it is not visible in this figure. In the strong forcing case, the low-frequency part of the spectrum is drastically changed. The 12 h cycle can now be seen (denoted by red circle). Still, the unforced frequency appears as a dominant mode.

Time-averaged velocity is similarly shown to persist despite the presence of tidal forcing. Figure 11 plots the average velocities from Figure 6c along with those of the corresponding tidally forced simulations (where, again, tidal amplitude is 1 m). The average velocities are nearly identical, despite the fact that the slip distance of individual events, as well as the timing of events, differ between unforced and tidally forced simulations.

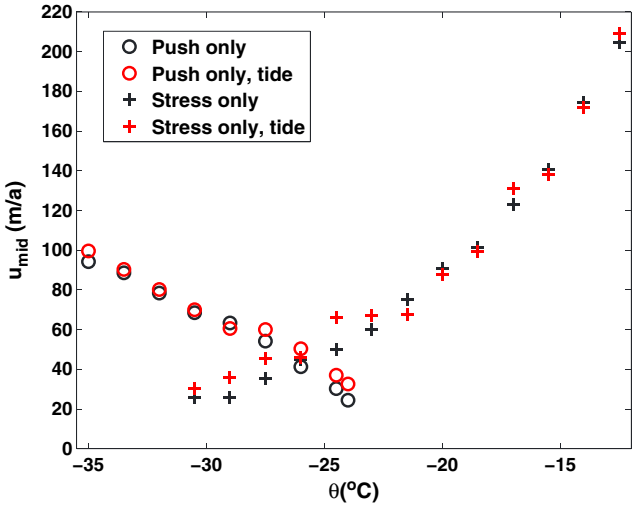

Figure 11. Tidally forced and unforced averaged velocities as functions of temperature in the stress-driven and push-driven models.

7. Discussion and Conclusions

Using a model of a viscoelastic ice stream with an idealized geometry and a simplified treatment of complex physics at the ice-bed interface, we were able to reproduce spatially variable stick-slip behavior similar to that observed on Whillans Ice Plain. Accounting for viscoelastic deformation allows us to join the elastic deformation recorded in stick-slip observations with the irreversible deformation characteristic of glacial movement on longer time scales.

Our experiments showed that ice viscosity (controlled through ice temperature) has an effect on the timing of slip events, and therefore on the time-averaged

contribution of stick-slip motion, and that this effect differs between stress-driven and push-driven stick-slip modes. More importantly, the results showed an apparent functional dependence of average velocity on temperature similar to that of steady sliding; analogous results were seen when varying stream width and driving stress. These functional dependencies may hold even in the presence of tidal forcing. Meanwhile, the parameters that determine velocities during slip events, such as elastic modulus (G) and bed relaxation time (T_b), were shown to have little influence on time-averaged velocities.

These results suggest that time-averaged velocity depends almost entirely on those parameters that determine flow in the case of purely viscous sliding: ice temperature, geometry, and driving stress. The exceptions are the bed strength parameters τ_s and τ_k, which influence both time-averaged and slip velocities. However, Figure 6c implies the existence of an "effective yield stress" which arises from the stick-slip cycle. No attempt was made to determine the value of this effective strength with our model; but our analytical solution in the supporting information suggests that it depends only on τ_s and τ_k, and not, for example, on elastic modulus or bed relaxation time.

If this time-averaged viscous response is a real feature of an ice stream or ice plain exhibiting stick-slip behavior, there are implications for estimation of basal behavior. As shown in section 5, viscous deformation should be accounted for in the inference of subglacial properties based on stick-slip observations. Meanwhile, satellite remote sensing provides velocities averaged over many stick-slip cycles; these are then used to invert for bed strength, assuming viscous ice deformation, even in areas known to exhibit stick slip [*Joughin et al.*, 2002]. With the use of viscoelastic models, these inverted "effective bed strengths" could be used to constrain the basal character of Whillans Ice Plain. Additionally, the result bolsters confidence that elastic stresses do not need inclusion in decadal- to millenial-time scale studies of ice stream flow, even ones that can potentially exhibit stick slip.

As was pointed out in section 2, the mechanism of rapid weakening of the ice-bed interface is largely unknown, and hence, we have chosen a simplified, phenomenologically based parameterization that does not imply a particular physical mechanism. However, it is important to establish that our results do not depend strongly on this choice. To address this, we have also implemented rate-and-state friction, a formulation commonly used to represent rock and granular friction. The experiments with the rate-and-state bed model are presented in the supporting information, with results qualitatively similar to those shown here.

Finally, it remains unknown as to why stick slip is unique to Whillans among the Siple Coast ice streams, even though others exhibit an elastic response to tidal forcing [e.g., *Anandakrishnan et al.*, 2003; *Walker et al.*, 2012]. The phenomenon could be because of differences in till character or related to Whillans deceleration [*Joughin et al.*, 2005]. Alternatively, it is possible that the extremely low driving stresses and weak bed of Whillans Ice Plain, even for the Siple Coast, allow small changes in bed strength to cause stick slip; a model such as ours could help assess this possibility. We anticipate that as increasingly comprehensive observations of the Whillans Ice Plain are made [e.g., *Winberry et al.*, 2011, 2013; *Pratt et al.*, 2014], and as the processes responsible for bed weakening become more clear, viscoelastic ice modeling efforts will aid in both quantifying these processes and in understanding the role of stick slip in glacial flow.

Appendix A: Numerical Solution

In order to satisfy equation (1) at time t_k, $u^{(k)}$ and $\tau_{xj}^{(k)}$ (the velocity and stress fields at time t_k) must be related to one another. If equation (1) is satisfied at time t_{k-1}, then equation (4) can be discretized (semi)implicitly in time:

$$\tau_{xy}^{(k)} - \tau_{xy}^{(k-1)} = \Delta t \left(G u_y^{(k)} - \frac{G}{\nu^{(k)}} \tau_{xy}^{(k)} + \epsilon \mathcal{N}_{xy}^{(k-1)} \right). \tag{A1}$$

Rearranging,

$$\tau_{xy}^{(k)} = \frac{G\Delta t}{1 + \frac{G\Delta t}{\nu^{(k)}}} u_y^{(k)} + \frac{1}{1 + \frac{G\Delta t}{\nu^{(k)}}} \tau_{xy}^{(k-1)} + \frac{\Delta t}{1 + \frac{G\Delta t}{\nu^{(k)}}} \epsilon \mathcal{N}_{xy}^{(k-1)}. \tag{A2}$$

Equation (3) is handled similarly. These expressions are inserted into the stress balance (1). The time-discretized stress balance becomes

$$\partial_y \left(\frac{G\Delta t}{1 + \frac{G\Delta t}{\nu}} u_y \right) - \frac{4}{R^2} \left(\frac{G\Delta t}{1 + \frac{G\Delta t}{\nu}} \right) u - \frac{1}{H} \tau_b^{\epsilon}(u) = \mathscr{L} \left(\tau_{\text{front}}, u_*, \nu, \tau_{xj}^{(k-1)}, u^{(k-1)} \right), \tag{A3}$$

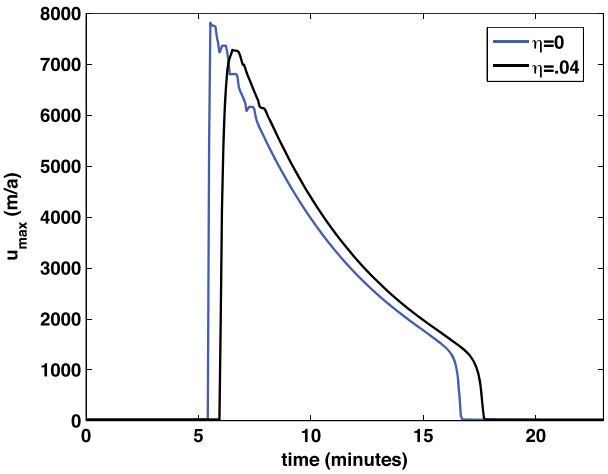

Figure A1. The effect of the damping term $-\eta u$. With nonzero η, nonphysical oscillations near the peak of the slip event are suppressed. The velocity profile is affected little otherwise.

where the superscript has been dropped for values at time t_k. The right-hand side, $\mathscr{L}$, is a lengthy expression not given here, but it does not depend on u or τ_{xj} at time t_k (except through ν). Since yield stress evolves on a time scale much longer than the time steps used in our model, τ_{yld} is lagged; i.e., τ_{yld}^{k-1} is used. It can be shown, using arguments similar to those of *Schoof* [2006, 2010], that equation (A3) has a unique solution (and further that the solution converges in the weak sense to the nonregularized plastic-bed solution as $u_\varepsilon \to 0$, although we do not vary this parameter). The equation is solved by finite differences, iterating on viscosity, ν, and the u in the denominator of equation (9). Once u is found at time t_k, τ_{xy}, τ_{xx}, and τ_{yld} can be stepped forward via equations (3), (4), and (8).

Equation (A3) is problematic in that it can lead to high-frequency, nonphysical oscillations in the velocity solution during slip events, particularly while velocities are highest. This may be due to the plastic formulation: on very short time scales (i.e., fractions of a second), velocity fluctuations do not affect ice shear stress, and since bed friction is not directly dependent on velocity, the velocity solution to equation (A3) can become numerically ill posed. The fact that a rate-and-state formulation does not lead to such difficulties (see the supporting information) supports this hypothesis. To avoid these spurious oscillations but also avoid long, costly iteration loops, a small damping term $-\eta u$ is added to the left-hand side of equation (A3). Figure A1 compares slip events of two experiments, differing only in the presence of the damping term; otherwise, the parameters are as in Figure 3. A value of 0.04 is used for η, which, in the finite-difference discretization of equation (A3), translates to a contribution of this magnitude to the matrix diagonal. Even though this term is roughly 0.1% of the other terms contributing to the matrix diagonal, it is enough to suppress the oscillations seen near the peak of the slip event. Aside from this, the damping term affects the solution very little. This same value of η is used in the experiments in the main text.

Appendix B: Timing of Slip Events

To interpret the timing of (nontidally forced) slip events, we develop an approximation for the interslip duration based on the equations; the result is then used to interpret the differing behavior at different temperatures observed in section 5. Based on the momentum balance, we relate scales of the different stress terms:

$$-\frac{H}{W}T_{xy} - \frac{2H}{L}T_{xx} + F = T_b, \tag{B1}$$

where T_{xy}, T_b, and T_{xx} are (time-dependent) representative scales of τ_{xy}, τ_b, and τ_{xx} just upstream of the ice plain, respectively. T_{xy} is defined to be positive, but T_{xx} can change sign over time. F represents the driving stress term that arises from longitudinal stress imposed downstream. T_{xy} and T_{xx} evolve according to

$$\dot{T}_{xy} = -\frac{G}{N}T_{xy}, \tag{B2}$$

$$\dot{T}_{xx} = -NE - \frac{G}{N}T_{xx}, \tag{B3}$$

where N is a representative scale for viscosity, which for simplicity we treat as uniform in time and space. E represents the forced longitudinal compressive strain rate due to upstream flow. These ordinary differential equations give

$$T_{xy} = T_{xy}^0 e^{-(t/T_M)}, \tag{B4}$$

$$T_{xx} = (T_{xx}^0 + NE)e^{-(t/T_M)} - NE, \tag{B5}$$

where T_M is the Maxwell time $\frac{N}{G}$ and T_{ij}^0 is the initial value of T_{ij}, which we take as the value at the end of the last slip event.

Equations (B4) and (B5) are inserted into equation (B1) to give an expression for T_b. T_b is then assumed to be equal to τ_k at time $t = 0$, and τ_s at the time t_s, the supposed time of the next slip event. (As was seen before, these bounds are not generally reached in an areally averaged sense, but still we make the assumption that the change in basal stress scales with $\tau_s - \tau_k$.) This yields equations which can be solved to find

$$t_s = T_M \log\left(\frac{\alpha_N - \tau_k}{\alpha_N - \tau_s}\right), \qquad \alpha_N \equiv 2HNE/L + F. \tag{B6}$$

α_N represents a sort of generalized driving stress scale, since it takes into account both driving factors (gravitational driving stress and upstream pushing).

The expression (B6) can be used to determine whether the stress loading rate of the bed should be approximately uniform over a range of values for the stress drop $\tau_s - \tau_k$, or whether the average loading rate should decrease with larger stress drops. A near-uniform loading rate implies the assumption of elastically deforming ice is appropriate, as discussed in section 5. Consider first the case where $\tau_s \ll \alpha_N$, i.e., where yield stress is much smaller than driving stress or the stress due to upstream compression. Since $\tau_k \leq \tau_s$, this leads to

$$t_s \sim T_M\left(\frac{\tau_s - \tau_k}{\alpha_N}\right), \tag{B7}$$

giving the result that the interslip duration scales with the stress drop of the bed, and the average loading rate remains constant when τ_s changes. While this is not exactly the same as having an elastic rheology—the expression (B7) depends on N if F is nonzero—it shows that a constant bed loading rate can be assumed when the bed strength is far below the generalized driving stress scale. As the sum of overall driving forces approaches τ_s, the bed loading becomes more nonlinear in time. This could come about because N is smaller, as in the warmer case shown in Figure 7.

Acknowledgments

D. Goldberg was supported by an NSF-OPP postdoctoral fellowship (ANT-1103375). C. Schoof was supported by a Natural Sciences and Engineering Council of Canada Discovery Grant and a Canada Research Chair. O. Sergienko was supported by NOAA grant NA13OAR431009. We thank reviewers J. Winberry and R. Bindschadler and one anonymous reviewer, Associate Editor J. Bassis, and Editor B. Hubbard for their constructive comments. We also acknowledge J. Rice, C. Wunsch, and M. Naylor for helpful conversations in the completion of this work.

References

Anandakrishnan, S., D. Voigt, R. B. Alley, and M. A. King (2003), Ice stream D flow speed is strongly modulated by the tide beneath the Ross Ice Shelf, *Geophys. Res. Lett.*, *30*(7), 1361, doi:10.1029/2002GL016329.

Bindschadler, R. A., P. L. Vornberger, M. A. King, and L. Padman (2003), Tidally driven stick-slip motion in the mouth of Whillans Ice Stream, Antarctica, *Ann. Glaciol.*, *36*, 263–272.

Brace, W. F., and J. D. Byerlee (1966), Stick-slip as a mechanism for earthquakes, *Science*, *153*(3739), 990–992, doi:10.1126/science.153.3739.990.

Bueler, E., and J. Brown (2009), The shallow shelf approximation as a "sliding law" in a thermomechanically coupled ice sheet model, *J. Geophys. Res.*, *114*, F03008, doi:10.1029/2008JF001179.

Catania, G., C. Hulbe, H. Conway, T. Scambos, and C. Raymond (2012), Variability in the mass flux of the ross ice streams, West Antarctica, over the last millennium, *J. Glaciol.*, *58*(210), 741–752, doi:10.3189/2012JoG11J219.

Chandler, D. M., R. I. Waller, and W. G. Adam (2005), Basal ice motion and deformation at the ice-sheet margin, West Greenland, *Ann. Glaciol.*, *42*(1), 67–70.

Danesi, S., S. Banniester, and A. Morelli (2005), Repeating earthquakes from rupture of an asperity under an Antarctic outlet glacier, *Earth Planet. Sci. Lett.*, *253*, 1151–158.

Dieterich, J. H. (1978), *Time-Dependent Friction and the Mechanics of Stick-Slip*, 790–806, vol. 116.

Fischer, U. H., and G. K. C. Clarke (1997), Stick-slip sliding behavior at the base of a glacier, *Ann. Glaciol.*, *24*, 390–396.

Gudmundsson, G. H. (2011), Ice-stream response to ocean tides and the form of the basal sliding law, *Cryosphere*, *5*(1), 259–270, doi:10.5194/tc-5-259-2011.

Hulbe, C. L., and M. A. Fahnestock (2004), West Antarctic ice-stream discharge variability: Mechanism, controls and pattern of grounding-line retreat, *J. Glaciol.*, *50*, 471–484.

Iverson, N. R. (2010), Shear resistance and continuity of subglacial till: Hydrology rules, *J. Glaciol.*, *56*(200), 1104–1114, doi:10.3189/002214311796406220.

Jellinek, H. H. G., and R. Brill (1956), Viscoelastic properties of ice, *J. Appl. Phys*, *27*, 1198–1209, doi:10.1063/1.1722231.

Joughin, I., S. Tulaczyk, R. Bindschadler, and S. F. Price (2002), Changes in west Antarctic ice stream velocities: Observation and analysis, *J. Geophys. Res.*, *107*(B11), 2289, doi:10.1029/2001JB001029.

Joughin, I., D. R. MacAyeal, and S. Tulaczyk (2004), Basal shear stress of the Ross ice streams from control method inversions, *J. Geophys. Res.*, *109*, B09405, doi:10.1029/2003JB002960.

Joughin, I., et al. (2005), Continued deceleration of Whillans Ice Stream, West Antarctica, *Geophys. Res. Lett.*, *32*, L22501, doi:10.1029/2005GL024319.

Kirchner, J. F., and C. R. Bentley (1979), Seismic short-refraction studies on the Ross Ice Shelf, Antarctica, *J. Glaciol.*, *24*(90), 313–319.

MacAyeal, D. R. (1984), Thermohaline circulation below the ross ice shelf: A consequence of tidally induced vertical mixing and basal melting, *J. Geophys. Res.*, *89*, 607–615, doi:10.1029/JC089iC01p00607.

MacAyeal, D. R. (1989), Large-scale ice flow over a viscous basal sediment: Theory and application to Ice Stream B, Antarctica, *J. Geophys. Res.*, *94*, 4071–4087.

Martin, M., R. Winkelmann, M. Haseloff, T. Albrecht, E. Bueler, C. Khroulev, and A. Levermann (2010), The Potsdam Parallel Ice Sheet Model (PISM-PIK), part II: Dynamical equilibrium simulation of the Antarctic Ice Sheet, *Cryosphere Discuss.*, *4*, 1307–1341.

Maxwell, J. C. (1867), On the dynamical theory of gasses, *Philos. Trans. R. Soc. London*, *157*, 49–88, doi:10.1098/rstl.1987.0004.
Paterson, W. S. B. (2001), *The Physics of Glaciers,* 3rd ed., Butterworth Heinemann, Oxford.
Pratt, M. J., J. P. Winberry, D. A. Wiens, S. Anandakrishnan, and R. B. Alley (2014), Seismic and geodetic evidence for grounding-line control of whillans ice stream stick-slip events, *J. Geophys. Res. Earth Surf.*, *119*(2), 333–348, doi:10.1002/2013JF002842.
Rathbun, A. P., C. Marone, R. B. Alley, and S. Anandakrishnan (2008), Laboratory study of the frictional rheology of sheared till, *J. Geophys. Res.*, *113*(F2), F02020, doi:10.1029/2007JF000815.
Reeh, N., E. L. Christensen, C. Mayer, and O. B. Olesen (2003), Tidal bending of glaciers: A linear viscoelastic approach, *Ann. Glaciol.*, *37*, 83–89.
Rosier, S. H. R., G. H. Gudmundsson, and J. A. M. Green (2014), Insights into ice stream dynamics through modeling their response to tidal forcing, *Cryosphere Discuss.*, *8*(1), 659–689, doi:10.5194/tcd-8-659-2014.
Rubin, A. M., and J. P. Ampuero (2005), Earthquake nucleation on (aging) rate and state faults, *J. Geophys. Res.*, *110*, B11312, doi:10.1029/2005JB003686.
Ruina, A. (1983), Slip instability and state variable friction laws, *J. Geophys. Res.*, *88*(B12), 10,359–10,370, doi:10.1029/JB088iB12p10359.
Schoof, C. (2006), A variational approach to ice stream flow, *J. Fluid Mech.*, *556*, 227–251.
Schoof, C. (2010), Coulomb friction and other sliding laws in a higher-order glacier flow model, *Math. Models Methods Appl. Sci.*, *20*, 157.
Schulson, E. (1999), The structure and mechanical behavior of ice, *21–27*, *51*(2), doi:10.1007/s11837-999-0206-4.
Sergienko, O. V., D. R. MacAyeal, and R. A. Bindschadler (2009), Stick-slip behavior of ice streams: Modeling investigations, *Ann. Glaciol.*, *50*(52), 87–94, doi:10.3189/172756409789624274.
Tulaczyk, S., W. B. Kamb, and H. F. Engelhardt (2000), Basal mechanics of Ice Stream B, West Antarctica. 1. Till mechanics, *J. Geophys. Res.*, *105*, 463–481.
Walker, R. T., K. Christianson, B. R. Parizek, S. Anandakrishnan, and R. B. Alley (2012), A viscoelastic flowline model applied to tidal forcing of Bindschadler Ice Stream, West Antarctica, *Earth Planet. Sci. Lett.*, *319–320*, 128–132, doi:10.1016/j.epsl.2011.12.019.
Walter, J. I., E. E. Brodsky, S. Tulaczyk, S. Y. Schwartz, and R. Petterson (2011), Transient slip events from near-field seismic and geodetic data on a glacier fault, Whillans Ice Plain, West Antarctica, *J. Geophys. Res.*, *116*, F01021, doi:10.1029/2010JF001754.
Wiens, D. A., S. Anandakrishnan, J. P. Winberry, and M. A. King (2008), Simultaneous teleseismic and geodetic observations of the stick-slip motion of an Antarctic ice stream, *Nature*, *453*, 770–775, doi:10.1038/nature06990.
Winberry, J. P., S. Anandakrishnan, R. B. Alley, R. A. Bindschadler, and M. A. King (2009), Basal mechanics of ice streams: Insights from the stick-slip motion of Whillans Ice Stream, West Antarctica, *J. Geophys. Res.*, *114*(F1), F01016, doi:10.1029/2008JF001035.
Winberry, J. P., S. Anandakrishnan, D. A. Wiens, R. B. Alley, and K. Christianson (2011), Dynamics of stick–slip motion, Whillans Ice Stream, Antarctica, *Earth Planet. Sci. Lett.*, *305*(3–4), 283–289, doi:10.1016/j.epsl.2011.02.052.
Winberry, J. P., S. Anandakrishnan, D. A. Wiens, and R. B. Alley (2013), Nucleation and seismic tremor associated with the glacial earthquakes of Whillans Ice Stream, Antarctica, *Geophys. Res. Lett.*, *40*(2), 312–315, doi:10.1002/grl.50130.
Zoet, L. K., S. Anandakrishnan, R. B. Alley, A. A. Nyblade, and D. A. Wiens (2012), Motion of an Antarctic glacier by repeated tidally modulated earthquakes, *Nat. Geosci.*, *5*, 623–626, doi:10.1038/ngeo1555.